A Novel Framework for Detecting Disaster-Induced Power Outages Globally via Satellite Observations

Prateek Arora[1,2,6], Luis Ceferino[2], and Gregory Dobler[3,4,5]

[1]Civil and Urban Engineering, New York University, Brooklyn, NY

[2]Department of Civil and Environmental Engineering, University of California, Berkeley, CA

[3]Joseph R. Biden, Jr. School of Public Policy and Administration, University of Delaware, Newark, DE

[4]Department of Physics and Astronomy, University of Delaware, Newark, DE

[5]Data Science Institute, University of Delaware, Newark, DE

[6]Correspondence Email: arorap@berkeley.edu

ABSTRACT

Power systems are vital to our society, yet they remain vulnerable to widespread damage from natural disasters, often resulting in large-scale outages. Satellite-captured nighttime lights offer a global-scale opportunity to map daily electricity use and detect power loss. Prior research has primarily relied on aggregating nightlight data over several days during disasters to compare with recorded power outages. However, the interpretation of daily, short-term nightlight variations to determine outages remains limited, hindering efforts to use this global dataset for timely outage mapping. Leveraging unique outage data, this study introduces a novel interpretation of nightlight intensity loss from buildings during outages to propose a two-stage framework that uses nightlight to predict power outages. First, a classification model is used to identify regions where the fraction of customers experiencing outages exceeds 0.05, thereby mitigating noise and cloud interference that could hinder the identification of extreme outages. Second, a regression model is used to predict outage fractions for high-outage cases to map out actual events utilizing our developed interpretation of nightlight loss. We train and validate our model using historical blackouts during

Hurricanes Irma (2017), Michael (2018), Ida (2021), and Ian (2022), each of which affected over a million customers. We show the model's generalizability using out-of-sample data from Hurricane Fiona (2022) in Puerto Rico. We also demonstrate the transferability of the framework to other disasters by tracking outages after earthquakes in Turkey (February 2023) and Myanmar (March 2025). The framework utilizes open-source, hazard-independent inputs to predict power outages worldwide, caused by various disasters, including earthquakes or ongoing conflicts, and even in regions without automated outage reporting.

INTRODUCTION

Power infrastructure forms the backbone of our society, and disruptions to electrical networks can deprive populations of critical services, such as healthcare, finance, and transportation. The US economy suffers annual losses of more than 100 billion dollars due to power outages (LaCommare and Eto 2004). These outages might be triggered by unintentional physical damage from natural disasters like Hurricane Ian (2022), which left 2.6 million customers without power (Florida Public Service Commission 2022). Alternatively, outages could occur due to intentional cyberattacks that target grid communication and control technologies (Avraam et al. 2023).

Power outage mapping is a valuable tool for utilities and emergency planners, allowing rapid response and efficient recovery of disrupted electrical networks. It can supplement manual outage reporting, especially in areas with communication breakdowns during disasters (Jim Giuliano 2020). Timely knowledge of outages enhances situational awareness, allowing utilities to assess the scale of disruption and respond proactively with targeted repairs to restore the power (Campbell 2012). Furthermore, identifying affected regions could enable the targeted delivery of emergency aid, such as medical supplies and food.

Beyond the immediate responses, mapping historical outages and their subsequent recoveries can reveal existing structural vulnerabilities in the grid, supporting long-term planning for grid resilience. Large structural systems such as buildings and bridges could be surveyed after months to observe structural performance during disasters (Sonmez et al. 2025; Ceferino et al. 2024) as recovery for such structures takes a longer time, up to years (Koliou et al. 2020). This extended

time period allows researchers to extensively study damages and develop fragility-based damage functions that link infrastructure performance to hazard intensity for future events.

In contrast, power infrastructure needs to be restored much earlier as it supports other critical infrastructure such as transportation, financial institutions, and healthcare (Gim and Miller 2022). Thus, we need tools and methods to document outages promptly to understand the coupled interaction between power infrastructure and natural hazards, thereby improving their understanding of grid vulnerability across different components of power systems (Arora and Ceferino 2023a). Moreover, integrating historical outages with probabilistic hazard analysis can identify regions most vulnerable to power outages during future natural disasters (Alemazkoor et al. 2020). These insights can inform policy and investments in mitigation interventions, such as grid hardening, targeting the regions with the greatest need. Finally, damage functions that relate power outages and hazard intensity would allow for an initial estimate of outages similar to building damage estimates available immediately after earthquakes (Wald et al. 2010).

Understanding the effects of natural disasters on electrical systems requires detailed records of power outages. In many regions, there is a lack of automatic metering infrastructure to report and document outages. Moreover, automatic reporting could be hindered during large-scale disasters due to damage to infrastructure (PowerOutage 2022). In addition, most utilities do not allow public access for power system and outage reports due to security concerns, as it exposes the vulnerabilities of the grid (National Academies of Sciences, Engineering, and Medicine 2017; U.S. Department of Energy 2022).

Satellite observations offer a globally scalable approach for mapping power outages and infrastructure vulnerabilities, especially in data-scarce or inaccessible regions (Román et al. 2019; Mitsova et al. 2024). Nighttime light imagery has been used to understand power loss during hurricanes (Montoya-Rincon et al. 2022), but its application to map actual outages remains limited. Most existing studies focus on long-duration disasters, aggregating nightlight imagery over several days (Azad and Ghandehari 2021; Mitsova et al. 2024), which limits their ability to capture the dynamics of short-term outages. Furthermore, prior studies have primarily quantified the percentage

change in nightlight intensity rather than quantifying outages. In (Cole et al. 2017), the authors used nightlight data to estimate outages based on the number of failed isolating devices, which required detailed information on power system components. Their analysis was limited to cross-validation for outages during Superstorm Sandy (2012) in Connecticut and Western Massachusetts. In contrast, our model is designed to be generalizable with power system independent variables across different geographies and events, making it globally scalable. The percent drop in nightlight intensity does not directly reflect actual outages due to inherent limitations, such as nightlights do not approach zero even for complete blackout, and uncertainties in nightlight retrievals due to cloud cover and various illuminating sources such as traffic lights (Román et al. 2019).

Machine learning and deep learning methods, including neural networks, have demonstrated significant potential for predicting disaster-induced power outages (Arora and Ceferino 2023b; Guikema et al. 2010; Wanik et al. 2017; Shashaani et al. 2018). In (Lebakula et al. 2024), authors leveraged nightlight imagery to also estimate the county-level population in the US using deep learning techniques. These advances highlight the potential of machine learning techniques to predict power outages using satellite-derived nighttime data. However, there is a need to understand the relationship between nightlights and power outages to model the power outages more accurately.

This paper first explores the relationship between attenuation of nightlights and power outages. Additionally, other factors, such as moon conditions, could also affect the detection of power outages. Thus, we include nightlight attenuation and additional parameters that can be related to power outages to develop a machine learning model for documenting power outages using satellite-based nightlights. To our knowledge, this is the first study to develop a physics-based interpretation of nightlight intensity loss with power outages and incorporate it into machine learning models to estimate the fraction of customers without power at the county level.

To develop model for percent customer outage using nightlights, we obtained county-level power outage data from (Brelsford et al. 2024) for major historical hurricane events, including Irma (2017) for Florida, Michael (2018) for Florida, North Carolina, and Virginia, Ida (2021) in Louisiana, and Ian (2022) in Florida to train and validate our model. We tested the generalization

of the model on out-of-sample outage observations from Puerto Rico following Hurricane Fiona (2022). We also present the results on documenting power outages caused by earthquakes in Turkey in February 2023 and Myanmar in March 2025. Finally, we present an example of developing an outage damage function by correlating satellite-derived outages with hazard intensity measures for Myanmar.

NIGHTTIME LIGHTS

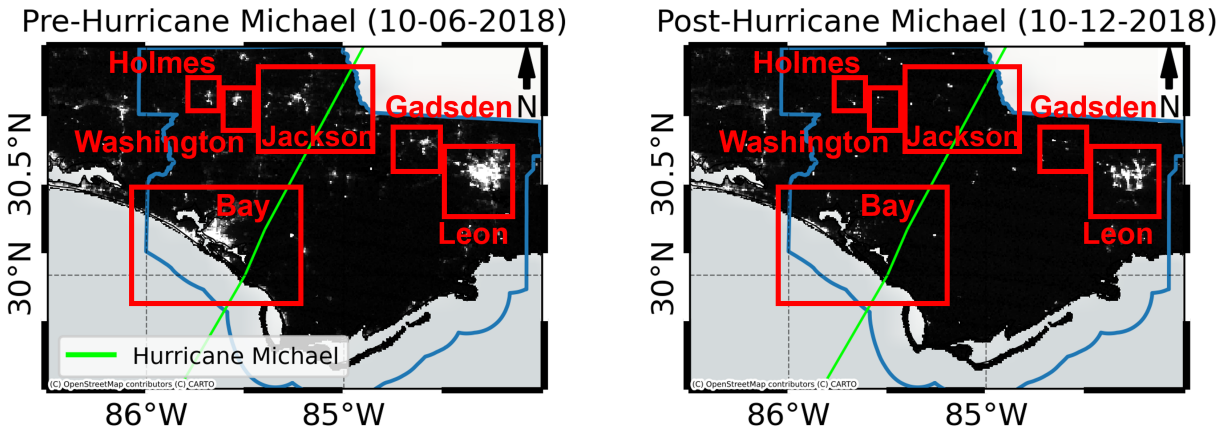

Fig. 1. Comparison of nightlight imagery before (left: October 6, 2018) and after (right: October 12, 2018) Hurricane Michael's landfall in Florida. A significant drop in nightlights is visible across the most affected counties (outlined in the figure), highlighting the widespread power outages caused by the storm.

The Suomi National Polar-orbiting Partnership (SNPP) is a sun-synchronous satellite equipped with the Visible Infrared Imaging Radiometer Suite, which includes a day/night band sensor that can capture nightlight imagery daily at a 500 m resolution (Román et al. 2018). For this study, we used the updated nightlight product-VNP46A2, corrected for the Bidirectional Reflectance Distribution Function, to account for varying illuminating conditions caused by moonlight and atmospheric conditions.

Previous research has demonstrated a correlation between post-disaster reductions in nightlight intensity and observed power outages at regional scales (Mitsova et al. 2024; Azad and Ghandehari 2021). For example, Figure 1 illustrates a significant drop in nightlight intensities across Florida's most affected counties following Hurricane Michael (2018), with reported outages approaching

90%. However, the observed decrease in nightlight intensity often does not exhibit a direct proportional relationship with the actual fraction of customers without electricity. For instance, due to the inherent properties of the sensor, nightlight data has a minimum detectable intensity threshold for valid measurements. This threshold prevents percent nightlight reductions from approaching zero, even for complete (100%) outages. Additionally, clouds obstruct satellite coverage, resulting in varying spatial coverage of building footprints and nightlight distributions. Thus, the direct percent difference between pre- and post-disaster nightlights might not accurately represent outage severity. This highlights the need for an interpretation of the relationship between nightlight intensity decay and outages.

Since SNNP sensors can introduce noise in nightlight observations, we aggregated intensity at the county level by summing across all pixels with the presence of at least one building. We utilize the Microsoft open building footprints within US (Microsoft 2018) and OpenStreetMap footprints from Humanitarian Data Exchange (Humanitarian Data Exchange 2014) for regions outside US. This minimizes noise and excludes lights from non-relevant sources, such as traffic lights. Additionally, some daily nightlight pixels within a county could be corrupted due to the presence of clouds or poor nightlight retrieval. We use the cloud flag and mandatory quality flag in VNP46A2 nightlight product to remove such affected pixels.

Previous studies have found a strong correlation between the varying urban land cover and total nightlight intensity (Cheon and Kim 2020). We explored the relationship between total daily nightlight intensity and building footprint in a county obtained from Microsoft building footprints (Microsoft 2018). Consistent with previous studies, we observe a linear relationship between the total building footprint and the aggregated nightlight intensity at the county level (Cheon and Kim 2020; Román et al. 2018). Figure 2 shows this trend for Bay County, Florida, where daily building footprints coverage correlates strongly in a linear trend with total nightlight intensity, except during the power outages caused by Hurricane Michael between 12 and 17 October 2018.

To account for varying satellite coverage, we define a normalized intensity metric (I) as the ratio of total nightlight intensity to total building footprint captured on a given day across a county (see

Methods). This normalized intensity metric is used to account for variability in building footprint coverage resulting from changing visibility conditions.

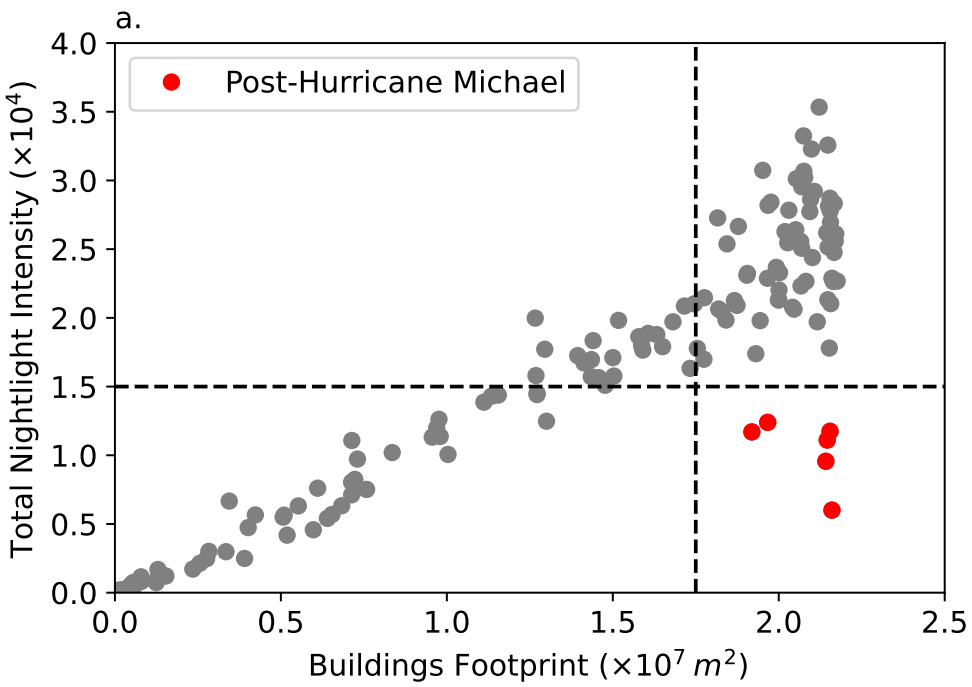

Fig. 2. Linear relationship between total nightlight intensity and building footprints in Bay County, Florida, from May 1 to October 31, 2018.

PHYSICS BASED FORMULATION FOR NIGHTLIGHTS

Previous research has modeled nightlight reductions from foliage cover using parametric forms analogous to Beer's Law, where observed intensity decreases exponentially with vegetation density (Román et al. 2018). We adopt a similar approach in which the ratio of post- to pre-disaster nightlight intensity at the county level decreases exponentially with the fraction of customers experiencing power outages (see Methods).

By analogy with light attenuation, we treat outage-affected areas as a medium that reduces the luminous sources. While outages are discrete events (e.g., individual buildings losing electricity) rather than a continuous medium, their aggregate effect on observed luminosity resembles attenuation. This analogy enables a tractable relationship between outage fraction (f_O) and nightlight reduction, which we model as a linear function in logarithmic space, i.e., $\log(I/\bar{I})$, where $\bar{I}$ is the

average normalized intensity across the 30 most recent cloud-free pre-disaster days. This physics-based analogous interpretation enables modeling a non-linear relation between nightlight loss and the extent of power outages.

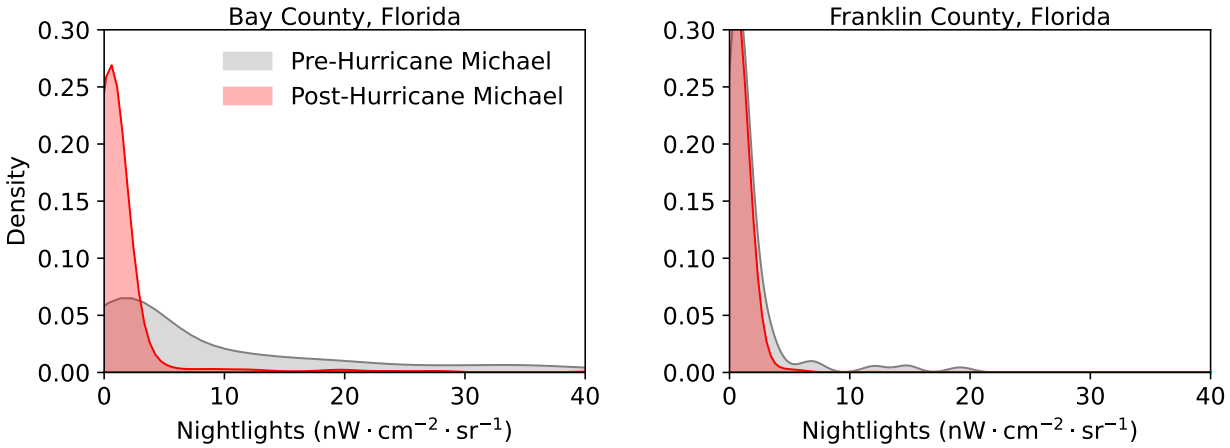

Fig. 3. Pre- and post-Hurricane Michael nightlight intensity distribution in Bay County and Jefferson County in Florida.

To observe and detect outages through nightlights, we must look for significant deviations in the nightlights during disasters. However, low-lit areas, such as sparsely populated rural counties with fewer buildings, capture nightlight intensity mostly close to the VIIRS sensor's threshold. Thus, such regions exhibit variations in nightlights across days due to noise from clouds and varying moonlight conditions, and significant deviations in nightlights after disasters are not observed. Figure 3 shows the distribution of nightlights in Bay County with a higher population density of 124 persons per square mile and Franklin County with a lower population density of 9 persons per square mile. In Figure 3, we observe significant deviations in nightlights across urban Bay County in pre- and post-Hurricane Michael (2018) satellite imagery, but deviations are insignificant in rural Franklin County. Hence, we focus on power outage detection in brighter regions with a population density of at least 25 persons per square mile.

High cloud cover can reduce satellite visibility and introduce uncertainties in nightlight values, potentially leading to underestimation or overestimation of power outages. To mitigate this, we include only those days when satellite observations cover at least one-third of the building footprint

and the land area in a county. For a robust baseline intensity estimation, we exclude days where I deviates by more than one standard deviation from $\bar{I}$. We further remove noisy observations where $log(I/\bar{I}) > 0.5$, and where $log(I/\bar{I}) > 0$ for fraction outages more than 0.2, as we expect negative $log(I/\bar{I})$ during power outages. After filtering, 2.2% outage data points were excluded, leaving 2,700 data points for training and validation. The 2,700 data points included 229 unique county-hurricane combinations, which we split into an 70:30 ratio, resulting in 1,936 training and 764 validation data points. We observe a strong Spearman correlation coefficient $|\rho|$ of 0.65 between $log(I/\bar{I})$ and the actual outage fraction, which highlights its utility as a strong predictive feature (Figure 4). To test the strong correlation between $\log(I/\bar{I})$ and f_O, we also examined alternative representations of nightlight decay, such as $I/\bar{I}$ and $\sqrt{I/\bar{I}}$, which showed correlation coefficients 15% and 8% lower, respectively, than that of $\log(I/\bar{I})$ with fractional outages.

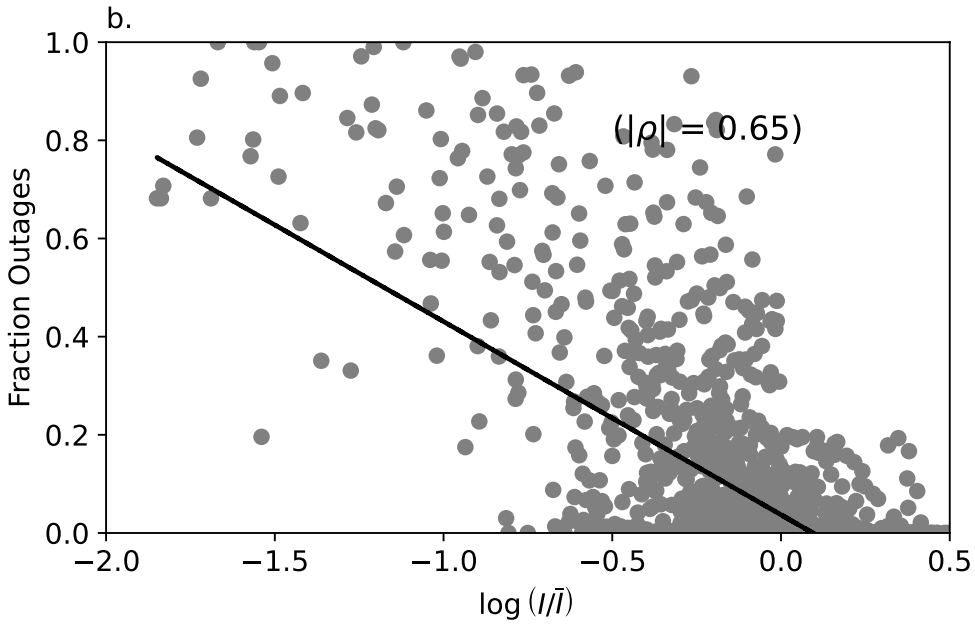

Fig. 4. Correlation between fraction of customers without power and $\log(I/\bar{I})$, showing Spearman's $|\rho| = 0.65$.

From Figure 3, urban areas exhibit significant deviations in nightlight distribution during outages, whereas rural regions show minimal deviations. This difference is likely due to the large energy consumption in urban areas, which drops significantly after a disaster. Thus, we include

a county's mean pre-disaster nightlight (L_M) as an explanatory variable to account for varying nightlight distribution across counties. This can help distinguish counties with low baseline nightlight and minimal observed post-disaster deviation, which may still experience significant outages.

We also included the proportion of the buildings' footprints covered by the satellite (f_p) within the pixels as input to the outage model. Regions with larger building coverage exhibit higher nightlight reductions during large outages, whereas areas with lower coverage may show lower or noisy deviations. Hence, including f_p captures the variations in nightlight intensities due to heterogeneity in structural densities. Additionally, building density (ρ_b) could indicate the distribution of vulnerable power systems (distribution lines and poles) in urban and rural areas (Arora and Ceferino 2023b). Significant differences could exist in the propagation and recovery of outages in gridded urban and radial rural grids. We also include ρ_b as input to the outage model to capture variations in grid topology.

Moonlight can affect the intensity of the nightlight captured by SNPP sensors. As reported by (Román et al. 2018), the intensity of nightlight varies with the illumination fraction of the moon. Thus, we also included the Moon fraction (M) as one of the inputs to correct the moonlight effects.

POWER OUTAGE MODELING FRAMEWORK

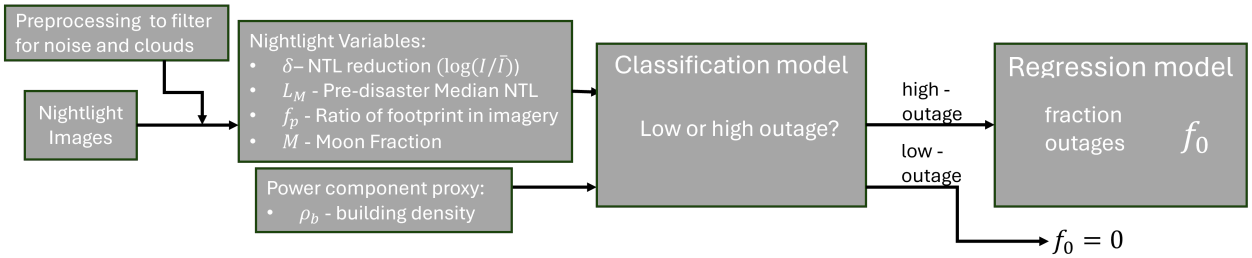

Fig. 5. Power outage modeling pipeline from acquiring nightlight imagery to predicting the fraction of customers without power.

We perform outage detection in two steps to address noise and data imbalance. Noise in nightlight intensity retrieval can introduce significant variability in intensity drop, especially when there are close to no outages. Furthermore, the data set is unbalanced, only $\sim$ 18.3% of the data

points have outages greater than 0.05. This imbalance could result in regression models overfitting to lower power outages. Since emergency responders and policymakers prioritize high-outage scenarios, it is crucial that the model correctly identifies and predicts high-outage scenarios.

To overcome noise and data imbalance, we first develop a classification model to distinguish between low- and high-outage days. Here, we define low outages as $f_0 < 0.05$ and high outages as $f_0 \geq 0.05$. Second, we develop a regression model to estimate the fraction of customers without power for days classified as high-outage events. Figure 5 presents the process of predicting outages using night-light imagery.

Previous studies have demonstrated the successful application of machine learning and deep learning techniques to estimate power outages across various hazards based on the physics-based intensity, such as winds of natural hazards (Nateghi et al. 2014). Here, we aim to develop a power outage model that captures the relationship between nightlight attenuation and the fraction of customer power outages applicable globally to predict outages at regional scales. Developed countries, such as the US, have outage monitoring systems, *e.g.,* EAGLE-I, to track outages. These systems are used by local utilities and planners for situational awareness and decision-making, especially when power systems are overwhelmed during disasters. The records of historical outage events could also be utilized to understand the impact of natural disasters on power systems, thereby anticipating and mitigating the consequences of future extreme events. Thus, a globally applicable power outage model could help local emergency management restore power outages in regions without outage monitoring, as power is necessary for the operation of emergency systems such as hospitals. This will also help plan resilient future grids more effectively.

To that end, we develop a machine-learning model that links reductions in highlights to power outages during natural disasters. Artificial neural networks (ANNs) can capture the nonlinear relationships and interactions among input variables, enabling more accurate modeling of power outages. We employ ANNs for classification and regression tasks to model the fraction of customers without power (f_O) as a function of the previously described input parameters (Figure 5).

However, in our efforts to also develop a simple and globally applicable power outage model,

we also present logistic regression to classify low and high outage events, and linear regression to predict outages for high outage events. We also compare the performance of logistic and linear regression combination to model outage against the ANNs-based model. Please see Methods for an explanation of both models.

Models Validation

Due to the class imbalance between low and high outage points, the classification model may overfit, primarily predicting low outages. To mitigate this, we randomly resampled low-outage cases to match the number of high-outage points, thereby training the classification model.

We used the *sklearn* library in Python to train and validate logistic and linear regression (Pedregosa et al. 2011). We used the Keras library in Python to build and train our Multi-Layer Perceptron (MLP) ANN models (Martín et al. 2015). We performed cross-validation to select the best architecture for classification and regression models of ANN with an input layer of a single hidden layer with five features, a single hidden layer with six neurons, and an output layer with only one output (see Methods and Supplementary Text S1). We use the Adam optimizer with a learning rate of 10^{-4} to train our models in mini-batches of 8 samples. We employed early stopping if the validation loss did not improve for 25 consecutive epochs, where one epoch represents a complete pass through the training data. We achieved the lowest validation loss for the classification model after 341 epochs and for the regression model after 1357 epochs.

We present the confusion matrix for logistic and ANN classification models on the testing data, which includes 616 points for low-outage events and 148 points for high-outage events, in Figure 6. The large difference in the number of low- and high-power outage data points represents the overall imbalance in power outage data, which is intuitive, as extreme power outage events are rare. We also present statistics on the classification models in Table 1. In Table 1, the accuracy means the ratio of events (either lower outage or high outage) classified correctly to the total events. The recall represents the ratio of the event classified correctly to the total instances of that event in the testing data. The precision represents the ratio of correctly classified events to the total number of cases of that event predicted on the testing data. Please also refer to the Methods section for the

confusion matrix and formulas for accuracy, recall, and precision.

We used the Keras library in Python to build and train our ANN models (Martín et al. 2015). We performed cross-validation to select the best architecture for classification and regression models of ANN with an input layer of a single hidden layer with five features, a single hidden layer with six neurons, and an output layer with only one output (see Methods and Supplementary Text S1). We use the Adam optimizer with a learning rate of 10^{-4} to train our models in mini-batches of 8 samples. We employed early stopping if the validation loss did not improve for 25 consecutive epochs, where one epoch represents a complete pass through the training data. We achieved the lowest validation loss for the classification model after 341 epochs and for the regression model after 1357 epochs.

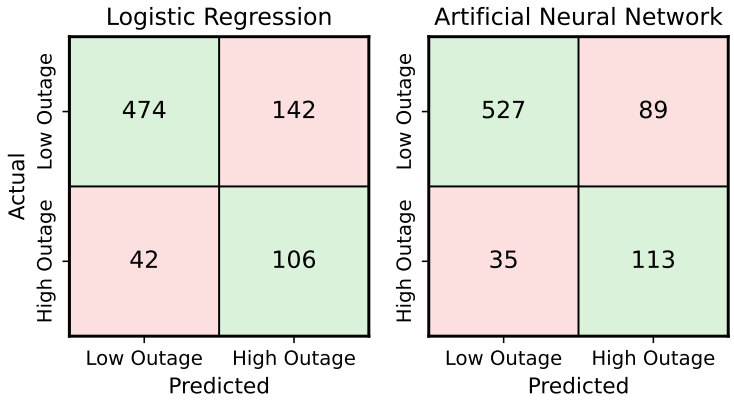

Fig. 6. Confusion matrix for logistic regression and ANN methods for classification of low and outage events.

All statistical performance metrics, including accuracy (75.9% for logistic regression and 83.7% for the artificial neural network), are comparable between the two models. Hence, we can also deploy logistic regression to capture high-outage events. However, both models exhibit relatively low precision (43% for logistic and 56% for ANN model) for high-outage predictions. This is primarily due to the class imbalance in the dataset, where low-outage events significantly outnumber high-outage events. Consequently, any misclassification of low-outage cases as high-outage cases disproportionately impacts precision. Given the importance of detecting high-outage events, we also emphasize recall for high-outages, which reached 71.6% on the validation dataset

for the logistic model. Thus, we can correctly identify 71.6% of the cases with high outages. Furthermore, the average outage for high-outage points misclassified as low outages is only 0.20 for logistic regression and 0.19 for the ANN classification model.

Additionally, the logistic regression classification model achieved an accuracy of 77.8% in the training data compared to 75.9% on the testing data. Similarly, the ANN achieved an accuracy of 80.5% on the training data compared to 83.7% on the testing data. The close agreement between training and validation performance suggests that our model generalizes well and is not overfitting.

We used the high-outage points ($f_O \geq 0.5$) in the training data to fit ANN and linear regression models. The linear regression model achieved an mean absolute error (MAE) of 0.14 on the training and validation datasets. The ANN regression model achieved an MAE of 0.12 on the training and 0.13 on the testing datasets. The linear regression model also shows comparable performance to the ANN regression model. Similar to classification models, linear regression models also do not overfit to the training data, as evidenced by comparable MAEs on training and validation datasets.

Model	**Accuracy**	**Precision**		**Recall**	
		Low Outage	High Outage	Low Outage	High Outage
Logistic Regression	75.9%	91.8%	42.7%	76.9%	71.6%
ANN	83.7%	93.7%	55.9%	85.5%	76.3%

TABLE 1. Comparison of classification models across performance metrics

We present the scatter plot on test data for the combined classification and regression models in Figure 7. We report weighted mean absolute errors (WMAE) for both models (see Methods) in Figure 7. WMAE is similar to MAE, but assigns greater weight to cases where actual high-outage points are misclassified as low-outage points, emphasizing the severity of missing major outages. In addition to demonstrating performance comparable to that of ANN models, logistic regression for classification and linear regression for predicting outage levels offer the advantage of being easily expressed through analytical equations. This enhances their interpretability and facilitates broader applicability across different geographic regions by using simplified equations. Here, we also present the classification and regression models in Figure 8 with coefficients of trained models, which can be used across different regions to predict the fraction of customers without power (f_O).

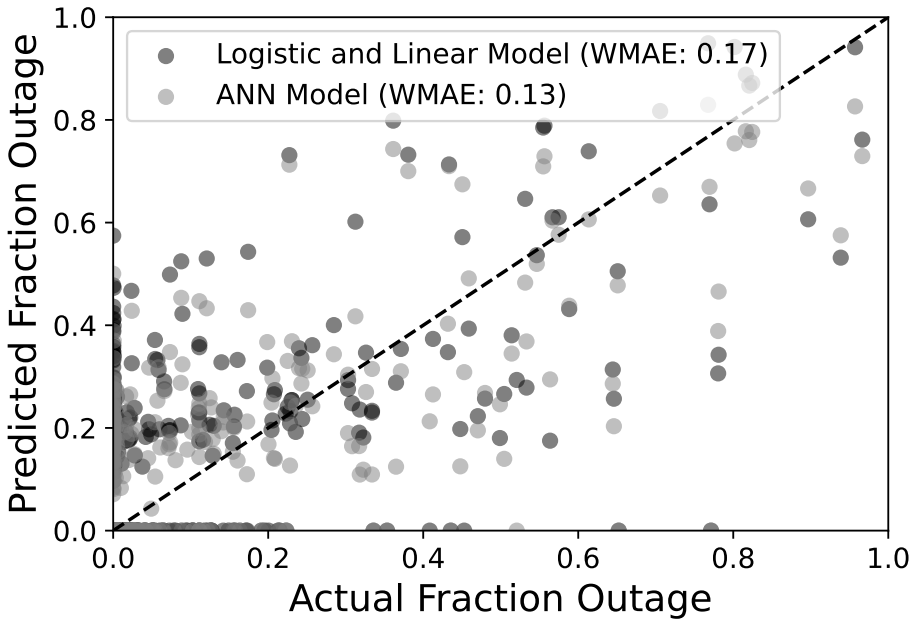

Fig. 7. Actual and predicted fraction of outages for the combined classification and regression models.

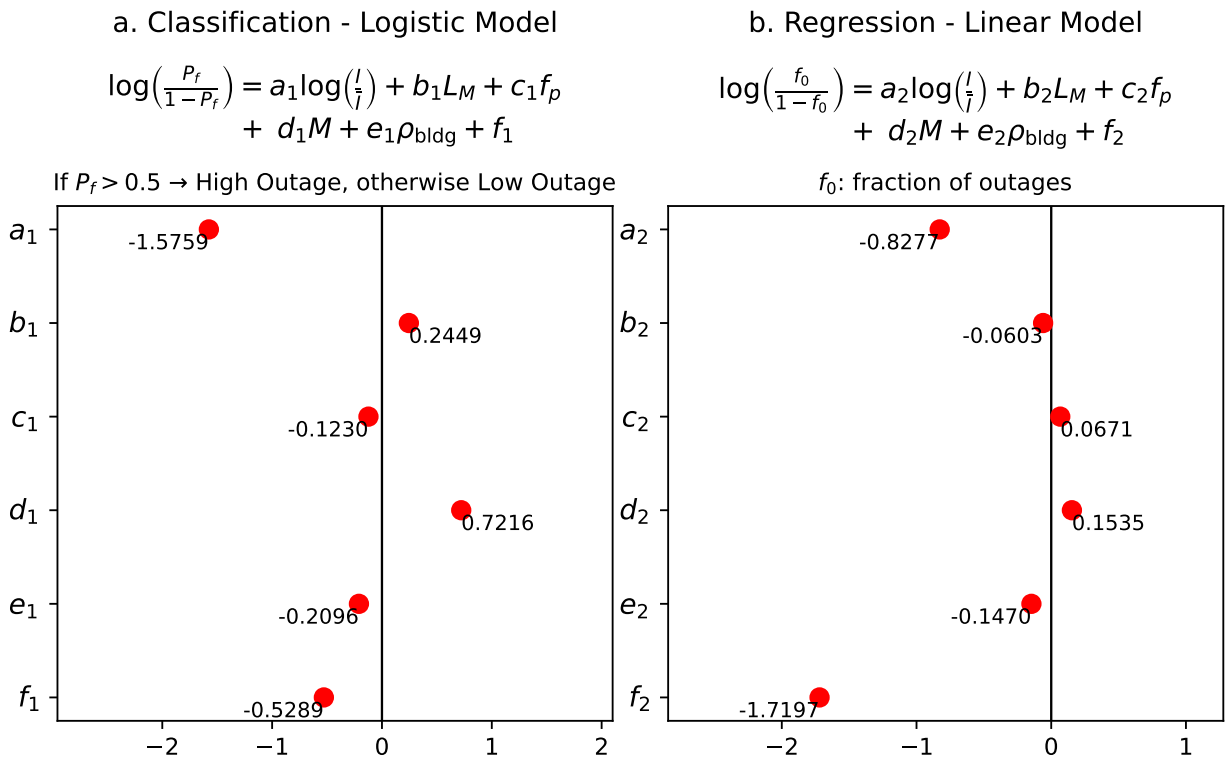

Fig. 8. Coefficients for the trained logistic regression and linear regression models.

The coefficients provided in 8 are for scaled features with zero mean and a standard deviation of one to avoid bias due to different scale of features (see Methods).

We find a negative coefficient for the decay parameter $\log(I/\bar{I})$, which indicates that outages increase as the decay parameter decreases. In contrast, a negative coefficient for building density represents that more populated urban areas with gridded power infrastructure are more robust to outages, which is consistent with the literature (Mitsova et al. 2018). We use a combination of logistic and linear regression models, as presented in Figure 8 to show the application of our developed model to detect power outages across several events.

DOCUMENT OUTAGES ACROSS EVENTS

Puerto Rico Outages During Hurricane Fiona (2022)

We evaluated our combined classification and regression models using Hurricane Fiona (2022), which made landfall in Puerto Rico on September 18, 2022. Figure 9a shows the predicted power outages using nightlight imagery with our developed approach, and Figure 9b presents a snapshot of the observed power outages reported by (PowerOutage 2022) on 25 September 2022, during the ongoing recovery of Puerto Rico communities. Note that the snapshot from (PowerOutage 2022) report discrete outage values (0.1, 0.3, 0.6, 1), whereas our model outputs continuous values from 0 to 1. Our model qualitatively captures the spatial pattern of extreme outages consistent with those reported by (PowerOutage 2022). In an effort to make a comparison between discrete outage values from (PowerOutage 2022) and our continuous, we classify the outages into four categories, i.e., low, medium, high, and severe. For the discrete case, we assign outages with 0.1 fractional outages to low, 0.3 to moderate, 0.6 to major, and 1.0 to severe category. For our continuous predictions, we assigned fractional outages less than 0.1 to low, between 0.1 to 0.3 to moderate, 0.3 to 0.6 to major, 0.6 to 1.0 to severe category. Extended Figure 1 presents the multiclass confusion for outages in 76 municipalities of Puerto Rico, excluding 2 municipalities with observations obscured by cloud cover. The overall accuracy of multiclass classification of outage levels across Puerto Rico is 62%. Furthermore, the severe outages had a recall of 86% and 70% of major outages are either classified

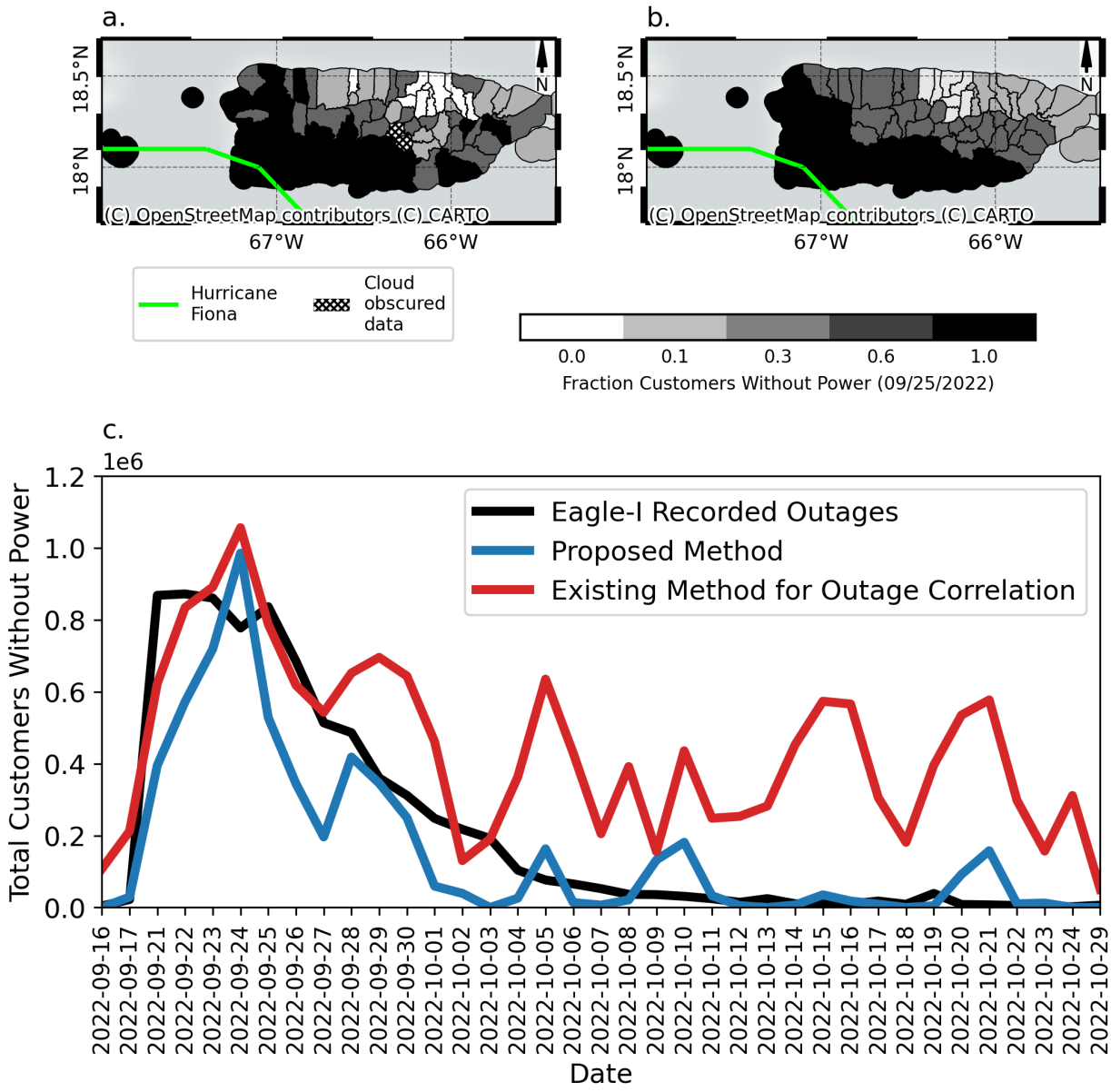

Fig. 9. a. Predicted fraction of customers without power in Puerto Rico on 09/25/2022 following Hurricane Fiona (2022). **b.** Snapshot of observed outages reported by (PowerOutage 2022). **c.** Power outage trajectories after Hurricane Fiona for Eagle-I recorded outages in black, proposed method (combined classification and regression models) in blue, and interpreted fractions of outages as the same as loss in nightlights in red. Initial satellite observations could be hindered by the formation of dense clouds during hurricanes.

as major or severe outages. The model shows potential to categorize and identify the most extreme outages.

Next, we obtained the power outage data for Puerto Rico during the storm from the EAGLE-I

dataset. The outages recorded in the EAGLE-I data set were available for seven health divisions encompassing Puerto Rico after Hurricane Fiona (2022) (Brelsford et al. 2024). These seven divisions include 78 municipalities (similar to counties) in Puerto Rico. The seven health divisions' scale and county-level predictions differ, but we still compare the total outages across Puerto Rico (Figure 9c). Due to the clouds obscuring the nightlights, power outage prediction is unavailable in all regions. Therefore, we assign these regions the mean fraction of customers without power for the available areas. We obtained total outages by multiplying the fractional outages in a municipality by the number of customers. Immediately after Hurricane Fiona (2022), there was no imagery due to clouds, so the outage peak was detected after a few days using nightlights. Our predicted recovery closely follows the actual recovery of Puerto Rico. We also present in Figure 9c the outages correlated as a percent change in mean nightlight across the municipality without any normalization with building footprint as referred in the literature (Montoya-Rincon et al. 2022). The peak of detected outages using our model has only 13% error compared to 21.1% error for outages correlating based on existing approach. Moreover, the existing approach consistently overestimates outages even during recovery, whereas our proposed method tracks the observed recovery trajectory more closely. Thus, our developed model can help detect the outages more accurately using nightlights.

The model could still occasionally predict zero outages despite reported outages. Such discrepancies could be addressed through temporal smoothing, *i.e.*, interpolating outage values on days with zero predictions if outages are predicted for adjacent days.

Outages in Turkey after the 2023 Earthquake

On February 6, 2023, Turkey experienced a devastating sequence of earthquakes that severely disrupted critical infrastructure across a wide region. The initial earthquake, a magnitude 7.8 event, struck at 1:17 UTC approximately 34 kilometers west of Gaziantep. This was followed by a powerful aftershock of magnitude 7.5 centered in Kahramanmaş Province (Ceferino et al. 2024). By February 23, 2023, more than 200 aftershocks were recorded in the region (Li et al. 2023). The districts of Antakya and Defne in Hatay Province, Turkey, especially suffered significant building

damage from these powerful earthquakes. Furthermore, on 20 February 2023, a 6.3-magnitude earthquake occurred in Hatay. This earthquake jolted southern Turkey, exacerbating the damage from the February 6 earthquakes (Sakarya et al. 2024).

There were no measures to track the damage to the power infrastructure after these massive earthquakes. Li et al. (2023) measured the communication network in the regions around the epicenters of above mentioned earthquakes. We utilize our outage models on nightlights to identify power outages in Turkey following the earthquakes. We used nightlight imagery to track the outages in heavily damaged districts of Antakya and Defne (Figure 10).

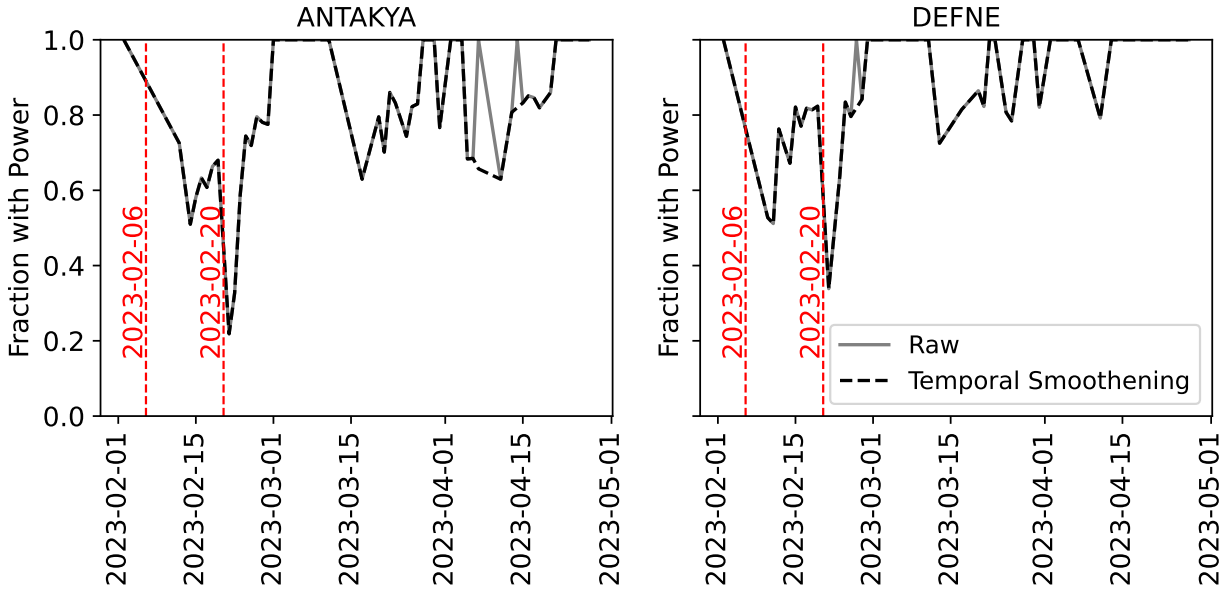

Fig. 10. Power outages tracked using our model in the districts of Antakya and Defne in Turkey after the February 2023 earthquakes.

Both regions exhibit a significant decline in the proportion of consumers with power following the earthquakes on February 6. Due to clouds, the first power outage prediction is available in Antakya on February 12, 2023, and in Defne on February 10, 2023. The peak fractional outage recorded with our model after the February 6 earthquakes is 0.46 in Antakya and 0.45 in Defne. Additionally, after the earthquake on 20 February, our nightlight-based model predicts peak fraction outage of 0.73 in Antakya and 0.61 in Defne. The Defne district shows quicker response to power outages than Antakya, which had suffered more damage. Our model predicts zero outages in Defne

on February 15th, which could be a false negative due to nightlight variation caused by clouds. This could also be due to recovery efforts, which could introduce extra lighting that could be mistaken for lights from buildings. Thus, we apply temporal interpolation to interpolate outages for days if the preceding and successive outage predictions were non-zero. On 15 March 2023, reports emerged of flash flooding in Turkey, which could have triggered power outages again in Antakya and Defne (Project HOPE 2023). Moreover, news reports the concerns about the unstable power supply in Antakya even months after the earthquake. Our proposed method can potentially capture the possible power outages during the worst-affected days across different hazards and different geographical regions.

Outages in Myanmar after the 2023 Earthquake

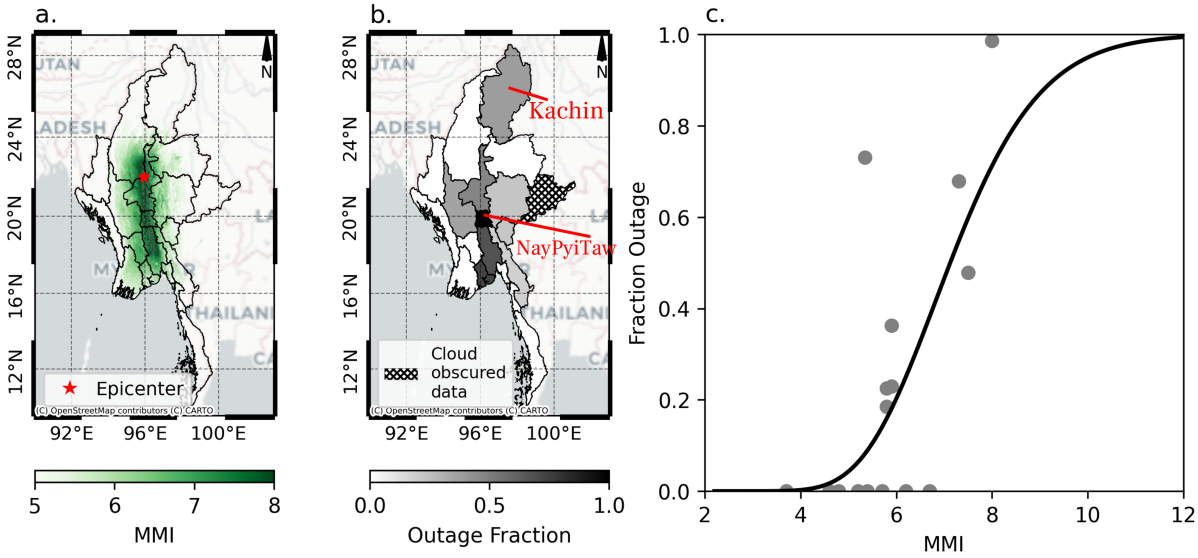

Fig. 11. a. MMI across Myanmar after the 7.7 magnitude earthquake on March 28, 2025. **b.**Spatial distribution of power outages across Myanmar as derived from satellite-based observations. **c.** Fragility curve showing the relationship between MMI and fraction outages.

On March 28, 2025, at approximately 12:50 p.m. local time in Myanmar, an earthquake of magnitude 7.7 struck near Mandalay, Myanmar's second-largest city. The earthquake was responsible for more than 3,500 fatalities and more than 5,000 injuries. The regions of Mandalay, Nayi Pyi Taw, and Magway suffered significant damage from the earthquake. USGS impact

summary of the event reports damage to more than 100,000 homes (U.S. Geological Survey nd).

There were reports of widespread outages after the earthquake throughout Myanmar (Shahzada et al. 2025). Furthermore, power outages began to recover the morning after the earthquake (POWERCHINA 2025). This provides an opportunity to document outages based on satellite-based observations. We used satellite imagery to predict outages in Myanmar on March 28, following an earthquake. In Figure 11, we show the distribution of Modified Mercalli Intensity (MMI) and predicted power outages after the earthquake. Our model predicted 99% outages in the Nay Pyi Taw region, 73% in Yangon, 67% in Bago (East), 48% in Mandalay, 36% in Magway, 23% in Kayah, 23% in Shan (South) and 19% in Kayin. These areas were the worst affected by the earthquake. Our model also predicted 39% outages in the Kachin region, which is not directly related to the earthquake but could be related to the conflict at the Myanmar Border (Council on Foreign Relations nd).

Historically, power outages resulting from natural disasters have not been well-documented. This provides an opportunity to understand the vulnerability of power systems at a global scale. Furthermore, documenting such outages could be utilized to develop damage functions similar to fragility curves developed for building damage. This would allow officials and emergency responders to identify the places in need and arrange for backups until the power is recovered fully. Here, we utilize our predicted outages (excluding the Kachin region as outages might be due to other conflicts) in Myanmar to fit a lognormal function to determine the fraction of outages as a function of MMI, presented in Figure 11c (Zentner et al. 2017) (see Methods). Note that the fragility curve for outages as a function of MMI is explicitly presented for the Myanmar region using our nightlight-based outage prediction model, other regions may exhibit different power grid vulnerabilities and consquently may have different fragility curve. Applying our model to nightlights to document historical outages during major natural disasters could help link disaster intensity (e.g., MMI for earthquakes) with outage patterns, allowing rapid assessment and timely deployment of emergency backups for severely affected regions. Additionally, fragility-based outage estimate in combination with probabilistic analysis, could identify the most vulnerable regions to future disasters, enabling

informed decisions on policies such as grid hardening, prioritization of infrastructure investments, and target emergency preparedness strategies (Arora and Ceferino 2023a).

DISCUSSION

This study demonstrates the utility of satellite-derived nightlight data for mapping power outages at a global scale. Identifying vulnerabilities in power infrastructure is a critical step toward enhancing system resilience and informing future grid planning efforts. Furthermore, this framework provides a foundation for rapid post-disaster assessment, particularly in data-scarce regions, by integrating satellite observations with infrastructure vulnerability analysis.

Previous research mostly interpreted outages directly as drop in nightlights (Montoya-Rincon et al. 2022) or utilized exclusive power system information with nightlights for a particular disasters to a limited geographic region (Cole et al. 2017), which limited the potential of nightlights to interpret outages at a global scale. We presented a novel framework with hazard- and power system- independent variables to estimate power outages using satellite-observed nightlight data. We modeled the attenuation of nightlight intensity in the logarithmic scale, which showed a good correlation ($|\rho| = 0.65$) with fraction of customers without power. Additionally, we incorporate building density as a proxy for the spatial distribution of power systems, enabling a more accurate estimation of outage impacts.

There is inherent noise in satellite observations due to clouds and nightlight retrievals at satellite sensor, particularly at fractional outage levels close to zero, and only 18.3% of the available data corresponds to outage fractions greater than 0.05, which limits the sample size for model fitting. To address the noise and data imbalance challenge, we developed an outage detection model using nightlights in two stages. First, we developed a classification model to classify low and high outage events with a boundary at 0.05 fraction of customers without power. Second, we developed a regression model to predict the fraction of customers without power for high outage events.

We developed logistic regression models for outage classification and linear regression models for predicting the magnitude of outages. Recognizing that artificial neural networks (ANNs) are capable of capturing complex nonlinear relationships, we also implemented ANN-based classifi-

cation and regression models. Our results showed that the combined use of logistic and linear regression models achieved performance comparable to that of ANN models on the test dataset. In addition to their comparable performance, these simpler models are easily expressed as mathematical equations, making them more accessible for global users seeking to apply satellite nightlight data for outage assessment.

We trained our model on major historical hurricanes, and the model performed well on the out-of-sample case of Hurricane Fiona (2022), demonstrating strong generalization. Our model showed a peak outage error of 13%, compared to 21.1% when outages were estimated using percentage changes only in nightlight intensity for Hurricane Fiona (2022). We also presented the case of Antakya and Defne, the worst-hit districts from the 2023 Turkey earthquakes. Both districts experienced outages following the initial earthquake on February 6, 2023, with the outages worsening after a 6.4 magnitude earthquake struck the Hatay region in southern Turkey on February 20, 2023.

We further extended our study to predict outages in Myanmar following the March 28, 2025, earthquake, which revealed a strong correlation with the Modified Mercalli Intensity (MMI) in Myanmar. Based on this analysis, we developed a lognormal fragility curve that relates the fraction of customers without power to MMI, supporting efforts toward rapid damage assessment following disasters. Similar regional fragility functions could be developed for other regions worldwide to strengthen disaster resilience.

Our approach relies on openly available and hazard- and power system-independent inputs, making it generalizable and adaptable to a wide range of outage scenarios. Although satellite observations immediately after a natural disaster may be limited by cloud cover, developing and refining historical damage functions based on hazard intensity can still support rapid assessments and improve the long-term risk assessment of power outages caused by extreme events. Additionally, long-term outage mapping can aid in post-disaster damage assessment, inform emergency response efforts, and provide insights into population displacement in severely affected regions.

METHODS

Outage Dataset

We obtained county-level power outage data from Oak Ridge National Laboratory Database (Brelsford et al. 2024) for major historical hurricane events, including Irma (2017) for Florida, Michael (2018) for Florida, North Carolina, and Virginia, Ida (2021) in Louisiana, and Ian (2022) in Florida for training and validating our model. Since nightlight imagery would be able to capture outages during nighttime, we averaged the reported outages from 9 p.m. to 4 a.m. local time for training, validation, and testing. Our prediction variable is the fraction of customers without power (f_O) in a given county. The dataset included 229 unique county-hurricane combinations, which we split into a 70:30 ratio, resulting in 1,936 training and validation and 764 testing data points. Since there is a limited number of data points for training and validation, we performed 10-fold cross-validation for hyper-parameter tuning (see Supplementary). Finally, we divided the 1,936 data points into a 90:10 ratio for early stopping of training for ANN to avoid overfitting of the model to the training data.

Normalized Nightlight Intensity

We define a normalized intensity metric as the ratio of total nightlight intensity to total building footprint captured on a given day across counties. This is formulated as,

$$I = \frac{\sum L_i}{\sum A_i}, \tag{1}$$

where L_i is nightlight intensity of the i^{th} pixel containing at least one building and A_i is the building footprint area (in sq. meters) in that pixel. The building footprints are obtained from Microsoft open building footprints for regions within US (Microsoft 2018) and OpenStreetMap footprints from Humanitarian Data Exchange (Humanitarian Data Exchange 2014) for regions outside US.

Nightlights Decay and Fractional Outages

Based on previous studies for attenuation of nightlights when passing through vegetation, we developed an analogous relationship for the decay of nightlights during power outages as,

$$\frac{I}{\bar{I}} \propto exp(-f_O) \tag{2}$$

Here, f_O is the fraction of customers without power, I is the normalized nightlight intensity on a given day (Eq. 1), $\bar{I}$ is the average normalized intensity across the 30 most recent cloud-free pre-disaster observations. We considered the 30 most recent cloud-free pre-disaster nights to define the baseline, as nightlight intensity can vary seasonally due to changing environmental conditions. Based on Eq. 2, we can model f_O as a linear function of nightlight intensity reduction in log space *i.e.,* $log(I/\bar{I})$.

Feature Scaling

Machine learning algorithms, especially those that use gradient descent methods to learn coefficients, are highly sensitive to the scale of different values. Variables with a higher order of magnitude can dominate the regression and result in unreliable coefficients. Thus, we used the standard scaler, i.e., converting values to have a mean of zero and a standard deviation of one based on the values of the variable present in the training set. For a variable v, scaling is given as

$$v_{\text{scaled}} = \frac{v - \mu_v}{\sigma_v} \tag{3}$$

where μ_v and σ_v are the mean and standard deviations for the variable. In Table 2, we present the variables' mean and standard deviation to scale the feature for future predictions.

Logistic and Linear Regression

Logistic regression is one of the most widely used methods for binary classification (Hastie et al. 2009), which defines a boundary between the two binary classes based on the inputs. The boundary separating two binary classes can be represented as

Feature	μ_v	σ_v
$\log\left(I/\bar{I}\right)$	-0.063	0.281
$L_M(nW \cdot cm^{-2} \cdot sr^{-1})$	10.516	10.955
f_p	0.029	0.036
M	48.364	37.193
ρ_b(building per sq. miles)	132.304	147.325

TABLE 2. Mean and Standard Deviation of Input Features

$$z = \left(\sum_{i=1}^{n} w_j x_{i,j}\right) + b \tag{4}$$

where $x_{i,j}$ are the inputs, w_j are the weights, b is the bias, i represents one geographic region, such as county and j represents the input parameters. The sigmoid function is applied to convert z in Eq. 4 to represent the probability of classes and output ranges from 0 to 1. The sigmoid function is given as:

$$S(z) = \frac{1}{1 + e^{-z}} \tag{5}$$

If the output is greater than 0.5, it is classified as a high outage event; otherwise, it is classified as a low outage event. The weights and biases for logistic regression are learned through minimizing the cross entropy loss. We apply Ridge Regularization (Hoerl and Kennard 1970) with $\lambda_c = 1$ to prevent overfitting to the training data which is given as.

$$L_c = \sum_{i=1}^{N} [y_{c,i} \log(S_c(x_i)) + (1 - y_{c,i}) \log(1 - S_c(x_i))] \tag{6a}$$

$$L_{c,reg} = L_c + \lambda_c ||w_i||^2 \tag{6b}$$

where N is the number of training samples, $y_{c,i}$ is one for high outages, otherwise zero, $S_c(x_i)$ is the probability output for high outages by the classification model, and w_i are the weights in Eq. 4. Here, we employ logistic regression to classify the day as a low outage ($f_O \leq 0.05$) or a high

outage ($f_O > 0.05$) in a county. For high outage events, we use a linear regression model to predict the percentage of customers without power.

Since the fraction of customers without power should be bounded between zero and one, we apply a transformation to our target variable. The transformation should be monotonic-increasing for one-to-one mapping and differentiable for smooth optimization to obtain the weights for linear regression (Dunn and Smyth 2018). Here, we use the logit transformation, as shown below.

$$g(f_O) = log\left(\frac{f_O}{1 - f_O}\right) \tag{7}$$

where $g(f_O)$ is the logit transformation of the fraction of customers without power. So, the linear regression is represented as.

$$g(f_O) = \beta_j x_{i,j} + c \tag{8}$$

where β_j and c are the coefficients for j^{th} input parameter and intercept of linear regression. The transformation $f_O = 1/(1 + e^{-g(f_O)})$ gives the final output as a fraction of customers without power. When applying the logit transformation on f_O in Eq. 7, it should be in the open interval, i.e., $0 < f_O < 1$. Without compromising generalizability and ensuring that our input variable in Eq. 7 lies in the open interval between zero and one, we introduce a slack variable, as in (Arora and Ceferino 2024).

$$\tilde{f_O} = \begin{cases} f_O + \epsilon, & \text{if } f_O = 0 \\ f_O, & \text{if } 0 < f_O < 1 \\ f_O - \epsilon, & \text{if } f_O = 1 \end{cases} \tag{9}$$

Similarly to (Arora and Ceferino 2024), we chose $\epsilon = 10^{-8}$, to ensure no significant impact on the precision of the predicted outages. Thus, we use $\tilde{f_O}$ from Eq. 9 in Eqs. 7 and 8 to obtain the fraction of customers without power using linear regression. Like Eq. 10b, we minimize the

regularized ridge loss $\lambda_r = 1$ in linear regression to prevent overfitting, which is given as:

$$L_r = \sum_{i=1}^{N} (g(f_{o,i}) - g(\hat{f}_{o,i}))^2 \tag{10a}$$

$$L_{r,reg} = L_r + \lambda_r ||\beta_i||^2, \tag{10b}$$

where N is the number of data points used to fit the linear regression, $f_{o,i}$ and $\hat{f}_{o,i}$ are the actual and predicted fraction of customers without power, $g(.)$ is the logit function in Eq. 7, and β_i are the weights in Eq. 8. We use the training data with values only above 0.05 for f_o to fit the regression model.

Artificial Neural Network

ANNs consist of multiple computational layers composed of single units, "neurons" that transmit information and learn non-linear patterns to perform classification and regression tasks (Haykin 1994). Furthermore, they can better model the interaction between the input parameters, such as the aggregated attenuation in nightlights and pre-disaster median nightlights, to predict outages with higher accuracy.

In this study, we employed a feedforward neural network architecture for both classification and regression tasks. Each layer in an ANN performs linear operations, where every input is connected to each output through learnable weights. A non-linear activation function is then applied element-wise to the output, which is essential for capturing the complex non-linear interactions between input and output variables. The operation performed for each layer of the neural network can be given as,

$$O = G(W \times I + b) \tag{11}$$

where O is the set of output vectors of length k_2, I is the set of input vectors of length k_1, W is the matrix of weight parameters of size $k_1 \times k_2$ with each corresponding to connection between one input and one output, b is the bias, and G is an activation function applied element-wise for each layer.

For both the classification and regression models, we used the rectified linear unit (ReLU) activation function in the hidden layer and the sigmoid activation function in the output layer. The ReLU function is given as.

given as

$$ReLU(x) = x, \text{if } x > 0 \text{ else } 0 \tag{12}$$

The sigmoid function maps inputs to a range between 0 and 1 as represented in Eq. 5. Similar to logistic regression, the classification ANN model represents the probability of high outages, with values above 0.5 indicating a high-outage day. The regression model predicts the fraction of customers without power in counties classified as high-outage regions.

The weights of neural networks are learned by minimizing a loss function. For classification, we used binary cross-entropy loss (L_c) in Eq. 6a. For the regression model, we use the Huber loss (L_h) (Gokcesu and Gokcesu 2021), given as,

$$L_h = \frac{1}{N} \sum \begin{cases} \frac{1}{2}(y_{r,i} - S_r(x_i))^2, & \text{for } |y_{r,i} - S_r(x_i)| \leq \delta, \\ \delta \cdot \left(|y_{r,i} - S_r(x_i)| - \frac{1}{2}\delta \right), & \text{otherwise.} \end{cases} \tag{13}$$

where $y_{r,i}$ is the true fraction of customers without power, and $S_r(x_i)$ is the predicted fraction of customers without power. The Huber loss function combines mean squared error (MSE) for small errors and mean absolute error (MAE) for large errors, making it robust to outliers. We chose $\delta = 0.05$ to handle the significant deviations from extreme outages.

There are multiple architectures possible for both classification and regression ANNs. We performed cross-validation to select the best architecture for our developed classification and regression models. Please see the details in the supplementary. The classification and regression models we developed include an input layer, one hidden layer with six neurons, and one output node, as this architecture resulted in minimum cross-validation error.

Model Performance Metrics

Confusion Matrix: A confusion matrix compares the model predictions with the actual observed values (Table 3). The diagonal elements of the confusion matrix represent correct classifications, while the off-diagonal elements represent misclassifications. In this study, we define low-outage events as "Negative" and high-outage events as "Positive". Accordingly, "True Positives" refer to events that are actually high outages and are correctly classified as high outages. "False Positives" refer to events that are actually low outages but are incorrectly classified as high outages. Similarly, "True Negatives" and "False Negatives" refer to correct and incorrect classifications of low-outage events, respectively.

	Predicted: Low Outage	**Predicted: High Outage**
Actual: Low Outage	True Negative (TN)	False Positive (FP)
Actual: High Outage	False Negative (FN)	True Positive (TP)

TABLE 3. Confusion matrix for binary outage classification

Accuracy: The ratio of the total number of correct classifications (both positive and negative) to the total number of events in the dataset. Accuracy is computed as given below.

$$\text{Accuracy} = \frac{\text{TP} + \text{TN}}{\text{TP} + \text{TN} + \text{FP} + \text{FN}} \tag{14}$$

Recall: The ratio of correct classifications for a given class to the total number of events in that class. Below, we report the recall for positive (high-outage) events. Similarly, recall can be calculated for negative (low-outage) events.

$$\text{Recall} = \frac{\text{TP}}{\text{TP} + \text{FN}} \tag{15}$$

Precision: The ratio of correct classifications for a given class to the total number of events predicted as belonging to that class. Below, we report the precision for positive (high-outage) events; similarly, precision can be calculated for negative (low-outage) events.

$$\text{Precision} = \frac{\text{TP}}{\text{TP} + \text{FP}} \tag{16}$$

Weighted Mean Absolute Error (WMAE): To evaluate the performance of the complete model, which combines classification and regression, we used WMAE to amplify the error for false negatives, *i.e.*, cases where high outages are classified as low outages (Shashaani et al. 2018). We can represent WMAE as

$$\text{WMAE} = \frac{1}{N} \sum_{i=1}^{N} w^{\mathbf{1}\{\text{FN}(i)\}} \, |y(x_i) - \hat{y}(x_i)| \tag{17}$$

where $\mathbf{1}\{\text{FN}(i)\}$ is one for false negative case otherwise zero, $y(x_i)$ are the true fraction of outages, $\hat{y}(x_i)$ are the predicted fraction of outages, N are the total number of testing data points., and we use $w = 10$ for our study based on the study from (Shashaani et al. 2018).

Outage Function for Earthquakes

we use our predicted outages in Myanmar to fit a lognormal function to determine the fraction of outages as a function of Modified Mercalli Intensity (MMI), presented in Figure 11c (Zentner et al. 2017) (see Methods), which can be presented as.

$$f_O = \phi \left(\frac{\ln \left(\text{MMI} \, / \, \overline{\text{MMI}} \right)}{\beta} \right) \tag{18}$$

where f_O is the fraction of customers without power, MMI is the observed intensity in a region, $\overline{\text{MMI}}$ is the median of fragility curve (*i.e.,* $f_O(\overline{\text{MMI}}) = 0.5$), and β is the dispersion parameter.

CONTRIBUTIONS

P.A., L.C., and G.D. conceptualized the framework for power outage detection using nightlight imagery. P.A. curated the outage and satellite data and trained the power outage models with suggestions from L.C. and G.D.. P.A. drafted the manuscript with inputs and edits from L.C. and G.D.

ACKNOWLEDGMENT

Prateek Arora was supported by the NYU Tandon School of Engineering Fellowship. This work was also supported in part through the NYU IT High Performance Computing resources, services, and staff expertise.

DATA AVAILABILITY

Code and Data used to train and validate the models have been deposited to NSF's DesignSafe Repository (Arora and Ceferino 2025), available at link https://doi.org/10.17603/ds2-a8cv-yc65

REFERENCES

Alemazkoor, N., Rachunok, B., Chavas, D. R., Staid, A., Louhghalam, A., Nateghi, R., and Tootkaboni, M. (2020). "Hurricane-induced power outage risk under climate change is primarily driven by the uncertainty in projections of future hurricane frequency." *Scientific Reports*, 10(1), 1–9.

Arora, P. and Ceferino, L. (2023a). "A performance-based probabilistic framework to model risk to power systems from hurricanes." *14th International Conference on Applications of Statistics and Probability in Civil Engineering*.

Arora, P. and Ceferino, L. (2023b). "Probabilistic and machine learning methods for uncertainty quantification in power outage prediction due to extreme events." *Natural Hazards and Earth System Sciences*, 23(5), 1665–1683.

Arora, P. and Ceferino, L. (2024). "A Quasi-Binomial Regression Model for Hurricane-Induced Power Outages during Early Warning." *ASCE-ASME Journal of Risk and Uncertainty in Engineering Systems, Part A: Civil Engineering*, 10(2), 04024027.

Arora, P. and Ceferino, L. (2025). "Power outage prediction utilizing satellite-based nightlights decay, <https://doi.org/10.17603/ds2-a8cv-yc65>.

Avraam, C., Ceferino, L., and Dvorkin, Y. (2023). "Operational and economy-wide impacts of compound cyber-attacks and extreme weather events on electric power networks." *Applied Energy*, 349, 121577.

Azad, S. and Ghandehari, M. (2021). "A study on the association of socioeconomic and physical cofactors contributing to power restoration after hurricane maria." *IEEE Access*, 9, 98654–98664.

Brelsford, C., Tennille, S., Myers, A., Chinthavali, S., Tansakul, V., Denman, M., Coletti, M., Grant, J., Lee, S., Allen, K., Johnson, E., Huihui, J., Hamaker, A., Newby, S., Medlen, K., Maguire, D., Dunivan Stahl, C., Moehl, J., Redmon, D., Sanyal, J., and Bhaduri, B. (2024). "A dataset of recorded electricity outages by United States county 2014–2022." *Scientific Data 2024 11:1*, 11(1), 1–13.

Campbell, R. J. (2012). "CRS Report for Congress Weather-Related Power Outages and Electric System Resiliency Specialist in Energy Policy Weather-Related Power Outages and Electric System Resiliency Congressional Research Service Weather-Related Power Outages and Electric System Resiliency Congressional Research Service.

Ceferino, L., Merino, Y., Pizarro, S., Moya, L., and Ozturk, B. (2024). "Placing engineering in the earthquake response and the survival chain." *Nature Communications*, 15(1), 4298.

Cheon, S. and Kim, J.-A. (2020). "Quantifying the influence of urban sources on night light emissions." *Landscape and Urban Planning*, 204, 103936.

Cole, T. A., Wanik, D. W., Molthan, A. L., Román, M. O., Griffin, R. E., Yu, B., Zhou, Y., He, C., Li, X., and Thenkabail, P. S. (2017). "Synergistic Use of Nighttime Satellite Data, Electric Utility Infrastructure, and Ambient Population to Improve Power Outage Detections in Urban Areas." *Remote Sensing 2017, Vol. 9, Page 286*, 9(3), 286.

Council on Foreign Relations (n.d.). "Rohingya crisis in myanmar. Accessed: 2025-05-25.

Dunn, P. K. and Smyth, G. K. (2018). *Generalized Linear Models With Examples in R, https://link.springer.com/book/10.1007/978-1-4419-0118-7*.

Florida Public Service Commission (2022). "Florida Public Service Commission, <https://www.floridapsc.com/>.

Gim, C. and Miller, C. A. (2022). "Institutional interdependence and infrastructure resilience." *Current Opinion in Environmental Sustainability*, 57, 101203.

Gokcesu, K. and Gokcesu, H. (2021). "Generalized huber loss for robust learning and its efficient

minimization for a robust statistics." *arXiv preprint arXiv:2108.12627*.

Guikema, S. D., Quiring, S. M., and Han, S. R. (2010). "Prestorm Estimation of Hurricane Damage to Electric Power Distribution Systems." *Risk Analysis*, 30(12), 1744–1752.

Hastie, T., Tibshirani, R., and Friedman, J. (2009). *The Elements of Statistical Learning: Data Mining, Inference, and Prediction*. Springer Series in Statistics. Springer, New York, 2nd edition.

Haykin, S. (1994). *Neural networks: a comprehensive foundation*. Prentice Hall PTR.

Hoerl, A. E. and Kennard, R. W. (1970). "Ridge regression: Biased estimation for nonorthogonal problems." *Technometrics*, 12(1), 55–67.

Humanitarian Data Exchange (2014). "Humanitarian Data Exchange: Find & Use Crisis Data. Accessed: 2025-08-09.

Jim Giuliano (2020). "Review and Assessment of Electric Utility Performance August." (1135), 1406489.

Koliou, M., van de Lindt, J. W., McAllister, T. P., Ellingwood, B. R., Dillard, M., and Cutler, H. (2020). "State of the research in community resilience: Progress and challenges." *Sustainable and resilient infrastructure*, 5(3), 131–151.

LaCommare, K. H. and Eto, J. H. (2004). "Understanding the cost of power interruptions to U.S. electricity consumers.

Lebakula, V., Datla, V., Wanik, D. W., and Cosby, A. G. (2024). "Predicting County-Level Population From VIIRS Nighttime Light Imagery With Deep Learning." *IEEE Sensors Journal*, 24(8), 13477–13487.

Li, X., Dimasaka, J., Zhang, X., Yu, X., Wang, C., Hu, X., Noh, H. Y., Zhao, X., and Xu, S. (2023). "M7.8 turkey-syria earthquake impact estimates from near-real-time crowdsourced and remote sensing data, <https://doi.org/10.17603/ds2-vnsc-y870>.

Martín, A., Ashish, A., Paul, B., Eugene, B., Zhifeng, C., Craig, C., Greg, S. C., Andy, D., Jeffrey, D., Matthieu, D., et al. (2015). "Tensorflow: Large-scale machine learning on heterogeneous systems." *Software available from tensorflow. org*, 7.

Microsoft (2018). "USBuildingFootprints: Computer Generated Building Footprints for the United

States. Accessed: 2025-08-09.

Mitsova, D., Esnard, A. M., Sapat, A., and Lai, B. S. (2018). "Socioeconomic vulnerability and electric power restoration timelines in Florida: the case of Hurricane Irma." *Natural Hazards*, 94(2), 689–709.

Mitsova, D., Li, Y., Einsteder, R., Roberts Briggs, T., Sapat, A., and Esnard, A. M. (2024). "Using Nighttime Light Data to Explore the Extent of Power Outages in the Florida Panhandle after 2018 Hurricane Michael." *Remote Sensing 2024, Vol. 16, Page 2588*, 16(14), 2588.

Montoya-Rincon, J. P., Azad, S., Pokhrel, R., Ghandehari, M., Jensen, M. P., and Gonzalez, J. E. (2022). "On the Use of Satellite Nightlights for Power Outages Prediction." *IEEE Access*, 10, 16729–16739.

Nateghi, R., Guikema, S., and Quiring, S. M. (2014). "Power Outage Estimation for Tropical Cyclones: Improved Accuracy with Simpler Models." *Risk Analysis*, 34(6), 1069–1078.

National Academies of Sciences, Engineering, and Medicine (2017). "Enhancing the Resilience of the Nation's Electricity System." *Enhancing the Resilience of the Nation's Electricity System*.

Pedregosa, F., Varoquaux, G., Gramfort, A., Michel, V., Thirion, B., Grisel, O., Blondel, M., Prettenhofer, P., Weiss, R., Dubourg, V., Vanderplas, J., Passos, A., Cournapeau, D., Brucher, M., Perrot, M., and Duchesnay, E. (2011). "Scikit-learn: Machine Learning in {P}ython." *Journal of Machine Learning Research*, 12, 2825–2830.

POWERCHINA (2025). "Powerchina's swift response restores power for myanmar earthquake relief (April). Accessed: 2025-05-27.

PowerOutage (2022). "POWEROUTAGE.US, <www.poweroutage.us>.

Project HOPE (2023). "Deadly flooding impacting earthquake survivors in türkiye, exacerbating need for support (March). Accessed: 2025-05-25.

Román, M. O., Stokes, E. C., Shrestha, R., Wang, Z., Schultz, L., Sepúlveda Carlo, E. A., Sun, Q., Bell, J., Molthan, A., Kalb, V., Ji, C., Seto, K. C., McClain, S. N., and Enenkel, M. (2019). "Satellite-based assessment of electricity restoration efforts in Puerto Rico after Hurricane Maria." *PLOS ONE*, 14(6), e0218883.

Román, M. O., Wang, Z., Sun, Q., Kalb, V., Miller, S. D., Molthan, A., Schultz, L., Bell, J., Stokes, E. C., Pandey, B., and Seto, K. C. (2018). "NASA's Black Marble Nighttime Lights Product Suite." *Remote Sensing of Environment*, 210, 113–143.

Sakarya, A., Akın, O., and Kılıç, A. (2024). "Investigating the damage from the february 6, 2023 earthquakes in terms of building characteristics in the antakya and defne districts of hatay province." *International Journal of Disaster Risk Reduction*, 112, 104783.

Shahzada, K., Noor, U. A., and Xu, Z.-D. (2025). "In the wake of the march 28, 2025 myanmar earthquake: A detailed examination." *Journal of Dynamic Disasters*, 100017.

Shashaani, S., Guikema, S. D., Zhai, C., Pino, J. V., and Quiring, S. M. (2018). "Multi-Stage Prediction for Zero-Inflated Hurricane Induced Power Outages." *IEEE Access*, 6, 62432–62449.

Sonmez, E., Eryilmaz Yildirim, M., Aydin, M. F., and Koroglu, F. B. (2025). "Seismic performance assessment of structural systems in the aftermath of the 2023 kahramanmaraş earthquakes: Observations and fragility analyses." *Earthquake Spectra*, 41(1), 198–218.

U.S. Department of Energy (2022). "Doe announces $12 million to enhance cybersecurity of america's energy systems. Accessed: 2025-05-25.

U.S. Geological Survey (n.d.). "M7.7 mandalay (burma, myanmar) earthquake. Accessed: 2025-05-25.

Wald, D. J., Jaiswal, K. S., Marano, K. D., Bausch, D. B., and Hearne, M. G. (2010). "PAGER—Rapid assessment of an earthquake's impact, <https://pubs.usgs.gov/fs/2010/3036/>. U.S. Geological Survey Fact Sheet 2010–3036, 4 p. Revised November 2011.

Wanik, D. W., Parent, J. R., Anagnostou, E. N., and Hartman, B. M. (2017). "Using vegetation management and LiDAR-derived tree height data to improve outage predictions for electric utilities." *Electric Power Systems Research*, 146, 236–245.

Zentner, I., Gündel, M., and Bonfils, N. (2017). "Fragility analysis methods: Review of existing approaches and application." *Nuclear Engineering and design*, 323, 245–258.

EXTENDED DATA

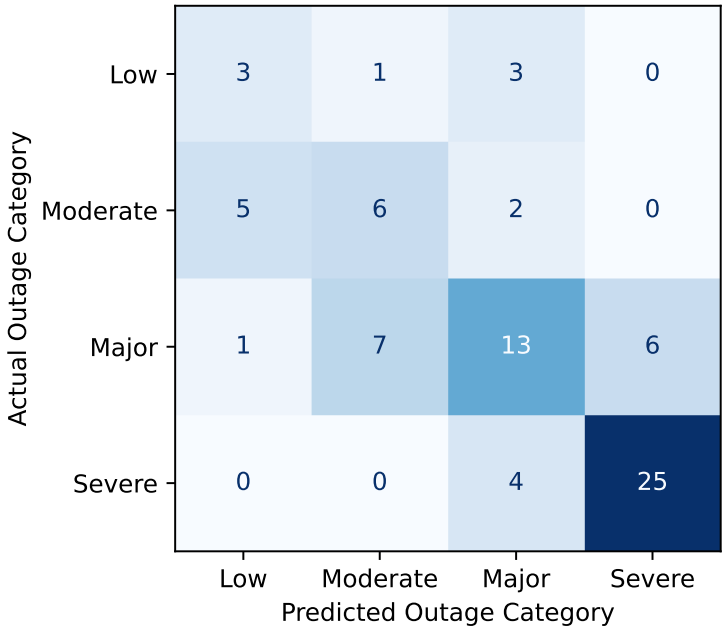

Extended Figure 1. Confusion matrix representing the outage categories across 76 municipalities for predictions on 09/25/2022 after Hurricane Fiona (2022) caused power outages across Puerto Rico.